RSC Advances

PAPER

View Article Online
View Journal | View Issue

Cite this: *RSC Adv.*, 2014, **4**, 22660

Fabrication of tunable Au SERS nanostructures by a versatile technique and application in detecting sodium cyclamate

Jing Chen,[ab] Wen Shen,[b] Biswajit Das,*[b] Yiyan Li[c] and Gaowu Qin*[a]

Received 12th February 2014
Accepted 16th April 2014

DOI: 10.1039/c4ra01243g

www.rsc.org/advances

In this work, three typical morphologies of SERS substrates with the compositions of Au nanoparticles, short Au nanowires (NWs) with small Au nanoparticles filled in the nanogaps and long Au NWs intertwined into a self-supporting film, were fabricated by a versatile nanocluster fabrication technique. This physical fabrication technique is easy to implement and cost-effective, and the fabricated SERS substrates have a large-area, good homogeneity and long-term stability. More importantly, the SERS substrates prepared by this physical method will not incorporate reductants and surfactant chemicals, and thus can yield clean surfaces, which are suitable for analytes with a weak affinity to the substrate surface. In this study, the fabricated substrate with the highest enhancement factor (EF) successfully acquired the SERS spectrum of sodium cyclamate, a restricted food additive, with a good signal–noise-ratio. Finally, a set of piece-wise linear equations were produced according to the correlation between SERS intensity and sodium cyclamate concentration with a detection limit of 1.6×10^{-9} M.

1. Introduction

Since its discovery, surface-enhanced Raman spectroscopy (SERS) has attracted great attention due to its significant enhancement capabilities.[1,2] Because SERS can provide an insight into the sharp and distinguishable vibrational structure of the molecules, together with its ultrasensitive and nondestructive detection property, it is an ideal approach for the detection of biological and chemical molecules.[3–18] Fabrication of reliable and highly enhanced SERS substrates is a necessary prerequisite for efficient SERS detection.

SERS substrates composed of nanoparticle, nanowire (NW) and nanofilm arrays are three typical SERS substrate patterns and have attracted great attention over the past decades.[19–25] Chemical synthesis has prevailed in producing nanoparticles and NWs. Strategies such as the self-assembly of nanoparticles into ordered nanoparticle arrays and the assembly of NWs into ordered thin films are popular procedures for organizing the chemically produced nanoparticles and NWs into the three typical SERS substrate patterns.[26–31] Wang *et al.*[32] described that drying a 10 μL droplet of cetyltrimethylammonium bromide (CTAB)-capped Au colloid solution on indium-doped tin oxide (ITO) glass resulted in the formation of highly ordered Au spherical nanoparticle arrays with sub-10 nm interparticle spacings. The as-prepared nanoparticle arrays display enormous near-field enhancement at the metallic junctions, and also exhibit high SERS activity, stability, and reproducibility. Tao *et al.*[33] employed the Langmuir–Blodgett (LB) technique to assemble aligned monolayers of silver NWs that are ~50 nm in diameter and 2–3 μm in length, with an area of over 20 cm^2. The silver NWs were produced using poly(vinyl pyrrolidone) (PVP) as the capping agent. These monolayers of aligned Ag NWs can be readily transferred to any substrate and exhibit excellent SERS performance in ultrasensitive detection and molecule-specific sensing. More recently, Chen and co-workers[34] reported an oil–water (two-phase) interfacial self-assembly process for fabricating aligned Ag NW films on solid substrates, which do not require extra pretreatment of either the surface of the Ag NWs or the solid substrate. The resultant Ag NW film exhibited highly sensitive and reproducible SERS performance. As (*v*) has been detected with single digit ppb sensitivity from actual arsenic-contaminated groundwater samples by this SERS substrate. Freer and co-workers[35] demonstrated a dielectrophoretic assembly method for assembling single nanowires on electrodes and achieved a 98.5% single nanowire yield on >16 000 electrode sites over an area of 400 mm^2. The balancing of surface, hydrodynamic and dielectrophoretic forces makes the self-assembly process controllable, and the self-limiting process makes low defect assembly possible. The controllability, low defects and the ability to position NWs precisely on a substrate make dielectrophoretic assembly a promising approach for fabricating high-quality SERS substrates.

[a]*Key Laboratory for Anisotropy and Texture of Materials (Ministry of Education), Northeastern University, Shenyang 110819, China. E-mail: qingw@smm.neu.edu.cn*
[b]*Nevada Nanotechnology Center, Howard R. Hughes College of Engineering, University of Nevada, Las Vegas, NV 89154-4026, USA. E-mail: dasb@unlv.nevada.edu*
[c]*Department of Electrical and Computer Engineering, University of Nevada, Las Vegas, NV 89154, USA*

The techniques used in the above-listed literature are ingenious, and the SERS substrates they fabricated showed high enhancement and good reproducibility. However, it is worth noting that for the chemical syntheses of nanoparticles and NWs, cumbersome procedures will be required to control nanoparticle sizes and shapes, and the aspect ratios of NWs. Moreover, the assembly of nanoparticles and NWs also require extra delicate techniques. In Zhang's work,[36] polyvinylpyrrolidone (PVP) and ascorbic acid were added into purified silver colloid solutions, and well-separated triangular silver nanoplates (SNPs) were produced. Then, by immersing the substrates with hydrophobic surfaces into the SNP solution for about 20 h, single-layer self-assembled SNP films were obtained. More importantly, nanoparticles and NWs produced by chemical approaches will inevitably incorporate reductants and surfactant chemicals, which are hard to remove and will interfere with SERS detection.[37–39] In our previous work, by controlling the pH values of alkaline glucose solution, three different Ag SERS substrates composed of monodispersed nanoparticles, nanoparticle-linked NWs, and a NW-weaved mesoporous membrane were fabricated.[40] The SERS substrates produced by the chemical method in our previous work[40] had relatively high enhancement factors (EFs), which could achieve microorganism identification at the single cell level. However, the substrate interference has to be subtracted from the SERS spectrum obtained from the analyte due to the chemical interference, which is not convenient for fast detection.

In this work, employing a physical method to fabricate three typical SERS substrates composed of nanoparticle, NW and nanofilm arrays is proposed. The physical fabrication technique will yield clean surfaces, and thus it is suitable for analytes with a weak affinity to the substrate surface. Moreover, the SERS spectra acquired from these clean substrates are reliable, which is crucial for SERS detection. Considering that Ag nanoparticles are unstable under ambient conditions since they oxidize easily, Au SERS substrates were produced in this work. Nowadays, most of the physical methods for producing nanoparticles face obstacles in terms of nanoparticle size, material, location, and choice of substrate.[41] Here, a versatile nanofabrication technique was applied, which can deposit nanoparticles of any material and can control the nanoparticle size distribution by applying a Quadruple mass filter (QMF) on any substrate.[41] The technique used in this work (deposition of nanoparticles directly onto the uncovered substrates) has a higher throughput and lower cost compared to the notable lithography technique, which makes this direct nanoparticle deposition technique suitable for the scaled-up fabrication of SERS substrates.[42] In addition, by only changing the instrumental parameters, three typical morphologies of SERS substrates (Au nanoparticles, short Au NWs with small Au nanoparticles filled in the nanogaps, and Au NW-weaved self-supporting films) were fabricated in a simple and time-efficient process.

Next, to evaluate the performance of the SERS substrates, sodium cyclamate was selected as the analyte. Sodium cyclamate is an artificial sweetener, which is used as an additive and is added to a variety of foods, drinks, cosmetics, and medicines. Once ingested, cyclamate is converted to a metabolite, cyclohexylamine, which is harmful and can cause adverse male reproductive effects, according to a series of experiments conducted on rats and dogs.[43–47] The acceptable daily intake for cyclamate has been set at 11 mg kg^{-1} by the Joint Expert Committee on Food Additives (JECFA) and at 7 mg kg^{-1} by the Scientific Committee on Food of the European Commission (SCFEC) (2000).[48]

The homogeneity and long-term stability of the SERS substrates were tested, and their EFs were calculated. By applying the SERS substrate with the highest EF, a SERS spectrum of 0.1 M of sodium cyclamate was successfully acquired; this SERS intensity is 10 times higher than the SERS intensity obtained from the dense Au film substrate prepared by a common physical fabrication method. Finally, an assessment of the concentration dependence was provided. This technique is easy to implement, and by only adjusting the parameters, three typical Au SERS substrates with clean surfaces can be fabricated, which are suitable for scaled-up fabrication and fast detection.

2. Experimental section

2.1 Chemicals and materials

Rhodamine 6G (R6G) (≥95.0%, analytical standard), sodium cyclamate (neat, analytical standard) and ethanol (analytical standard) were purchased from Sigma-Aldrich, and were used directly without further purification. Gold target (2.00″ diameter × 0.125″ thick, 99.99%) was purchased from Kurt J. Lesker Company (CA, USA). Silicon wafers were purchased from Silicon Valley Microelectronics (SVM, CA, USA). Ultrapure water (18.2 MΩ cm) was used for the preparation and dilution of R6G solution and sodium cyclamate solution.

2.2 Au SERS substrates fabrication technique

Here, we used a nanocluster deposition system (NanoSys 2, Oxford Applied Research Inc.), which incorporated three parts: (1) the nanocluster source, (2) the QMF and (3) the main deposition chamber. These are further explained. (1) The schematic of the nanocluster source is shown in Fig. 1a. The nanocluster source consists of a DC magnetron discharge to produce nanoparticles, an aggregation region between the magnetron and the aperture to let the nanoparticles form nanoclusters, and an aperture through which the nanoclusters can enter into the QMF. There are several parameters that can be adjusted to vary the nanocluster size such as the power supplied to the magnetron, the rate at which the aggregation gases flow, the aperture size, and the distance between the magnetron and the aperture (variable using a linear drive).[49] The sputtering power was set at 115 W for fabricating all the SERS substrates in this work, which was a moderate value for this system and could generate an appropriate sputtering rate. (2) The QMF is positioned at the exit of the nanocluster source to measure and select the cluster mass produced by the source. The QMF consists of four rods. A voltage with a dc and ac component was applied to one pair, and a negative voltage was

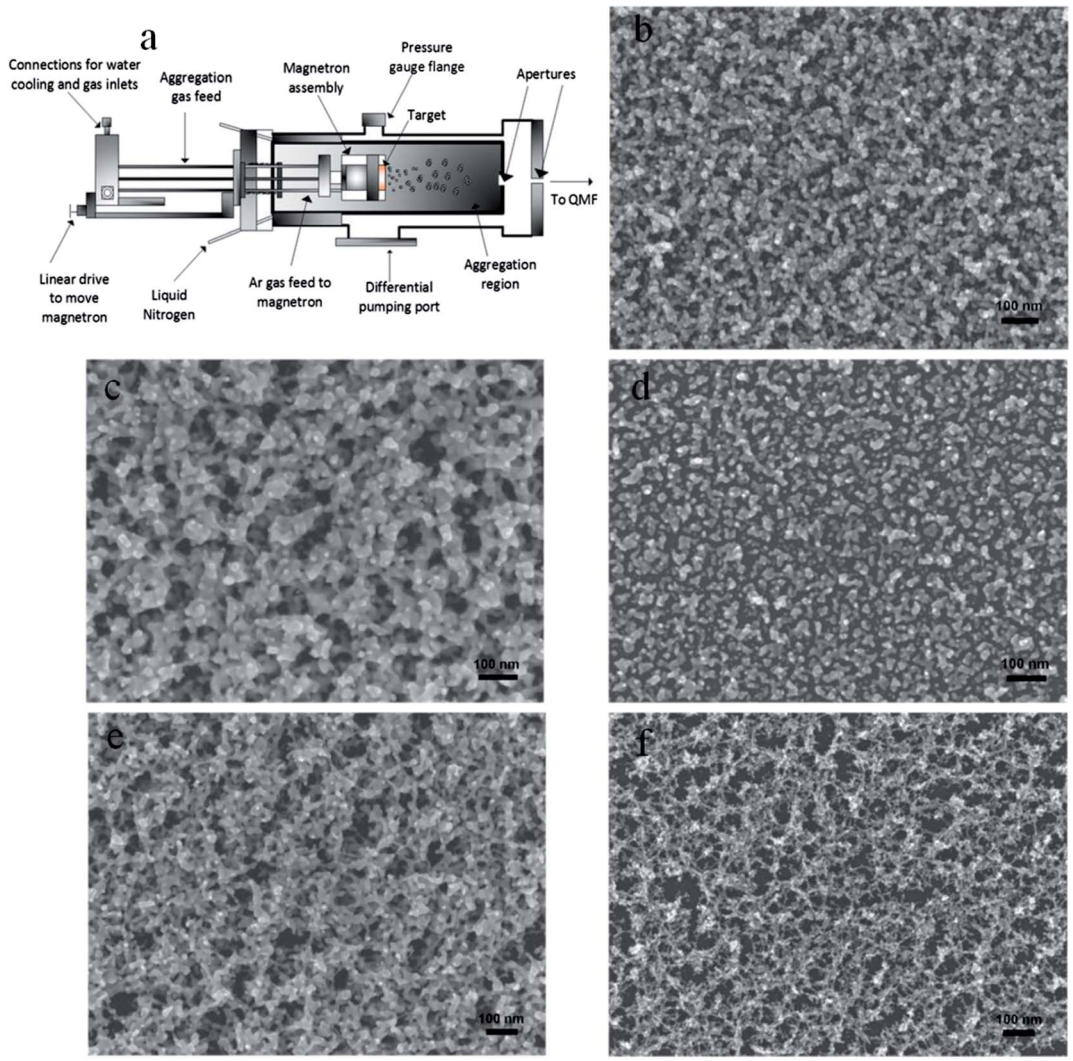

Fig. 1 (a): Schematic diagram of the nanocluster source.[41,49] (b) FE-SEM image of the Au SERS substrate fabricated with the QMF turned on and where the selected nanocluster size is 10 nm, the flow rate of Ar is 100 sccm and of He is 30 sccm, and the deposition time is 90 s. FE-SEM images of the Au SERS substrate fabricated with the QMF turned off, the flow rate of Ar is 100 sccm and of He is 30 sccm, and the deposition time is (c) 90 s, (d) 30 s. FE-SEM images of the Au SERS substrate fabricated with the QMF turned off, the flow rate of Ar is 100 sccm and of He is 0 sccm, and the deposition time is (e) 90 s, (f) 30 s. The sputtering power and aggregation length were all set at 115 W and 50 mm, respectively, for (b)–(f).

applied to the other pair. The nanoclusters produced by the source with various sizes entered into the QMF and moved along the axis of the rods. The nanocluster ions were selected according to their mass to charge (m/z) ratio, and ionized clusters with different m/z ratios followed different trajectories because of the quadrupole electric field, so that only ions with certain mass could be transmitted to the ion detector plate, and thus fulfilled the nanocluster size filtration.[41,49] There are several parameters which can influence the nanocluster size to pass through, these are the dc component U, the ac component V, and the frequency. The ratio U/V, called the resolution, determines the width of the nanocluster mass band transmitted through the filter. (3) The main deposition chamber, in which the substrate is mounted. Silicon wafer treated with piranha solution (concentrated H_2SO_4 : 30% H_2O_2 = 3 : 1 volume ratio. **Caution**: Piranha solution is extremely corrosive) was used as the substrate in this work.

A dense gold film was also produced by employing a common physical fabrication technique (sputter coating, 40 mA, 150 s) as a control substrate.

All the abovementioned substrates were stored separately in a commercial aluminum foil to prevent contamination, and kept in the dark at room temperature prior to use. The commercial aluminum foil was rinsed with ethanol and ultrapure water in advance for degreasing.

2.3 Substrate homogeneity and enhancement capability measurement

10 μL of 10^{-4} M R6G solution was dripped onto the three different Au SERS substrates. The SERS spectra were acquired immediately after the substrates were dried under ambient conditions. A normal Raman spectrum of 10^{-2} M of the R6G solution was also acquired.

2.4 Long-term stability measurement of SERS substrates

After 110 days, three Au SERS substrates were carefully taken out of the commercial aluminum foil to test their SERS performance. R6G was employed as the probe molecules, and 10 μL of 10^{-4} M of R6G solution was dripped onto each Au SERS substrate.

2.5 Preparation of sodium cyclamate solution

The initial concentration of sodium cyclamate was set at 10^{-1} M and was serially diluted to 10^{-9} M.

2.6 Characterization

The morphologies of the Au SERS substrates were observed by JEOL 7500F field emission scanning electron microscopy (FE-SEM). All SERS and bulk spectra were obtained using a confocal Horiba Jobin Yvon LabRAM HR Raman spectrometer equipped with a 785 nm laser and a 100× objective to focus the laser onto the sample surface and to collect the scattered light from the samples. The incident laser power was attenuated to 0.8 mW or 8 mW for SERS detection, and the laser power for the normal Raman spectra acquisition of 10^{-2} M bulk R6G solution was set at 80 mW. The frequency of the Raman instrument was calibrated by reference to a silicon wafer at a vibrational band of 520 cm^{-1}. All the measurements were carried out under ambient conditions.

3. Results and discussion

3.1 Fabrication and characterization of three kinds of Au SERS substrates and clarification of the forming mechanism

3.1.1 Au nanoparticles. First, we turned on the QMF, set a series of parameters to enable the nanoparticle size of around 10 nm pass through and reach the silicon wafer substrate. The sputtering power was 115 W. The flow rate of one of the aggregation gases Ar was 100 standard-state cubic centimeter per minute (sccm), and for the other aggregation gas He was 30 sccm. These two aggregation gases were used to cool and sweep the Au atoms and nanoclusters from the aggregation region to the aperture. The distance between the magnetron and the aperture was set at 50 mm, and the deposition time was 90 s. The FE-SEM image of the Au SERS substrate obtained under these parameters is shown in Fig. 1b.

Fig. 1b shows that the Au SERS substrate fabricated under the abovementioned parameters is composed of Au nanoparticles with a mean grain size of about 9–11 nm. The nanoparticles are of high density and are very close to each other, which is a good pattern for Raman enhancement since the extremely intense electromagnetic fields are expected at the sites of directly adjacent metallic nanostructures and not from single isolated metallic nanostructures. Because the QMF was on, only nanoparticles with a size around 10 nm could pass through the aperture and reach the Si substrate.

3.1.2 Au NW–Au nanoparticle conjugations. Subsequently, we turned off the QMF. The sputtering power was 115 W. The flow rate of one of the aggregation gases Ar was 100 sccm, and for the other aggregation gas He was 30 sccm. The distance between the magnetron and the aperture was set at 50 mm, and the deposition time was 90 s. The FE-SEM image of the Au SERS substrate obtained under these parameters is shown in Fig. 1c.

Fig. 1c shows that the Au SERS substrate is composed of short Au NWs with some small Au nanoparticles filled in the nanogaps formed by the NWs connecting to each other. The generated Au nanoparticles move along the aggregation region, while colliding and connecting to each other; thus, Au NWs are formed in the nanocluster source. Because the QMF was turned off, the NanoSys 2 did not participate in the filtration and selection of nanocluster size, which implied that Au nanoclusters of all sizes could pass through the aperture and reach the Si substrate.

To further verify and achieve a better clarification of this SERS substrate morphology, we shortened the deposition time (t = 30 s), but maintained the other parameters. The corresponding FE-SEM image is shown in Fig. 1d. When the deposition time becomes shorter, the silicon wafer substrate only has one layer of Au nanoclusters, which allows a better view. We can clearly see that the SERS substrate fabricated under these parameters is composed of short Au NWs (the aspect ratio is about 30–100 nanometers long and 20 nanometers wide) and with small Au nanoparticles (the mean grain size is about 9 nm) distributed around the NWs. As the deposition time becomes longer, these short Au NWs intertwine with each other and form a nanoporous film with small Au nanoparticles filled in the nanogaps, which is an ideal model for SERS enhancement.

3.1.3 Au nanofilm. Next, we changed the parameters and obtained another kind of SERS substrate. Again, we turned off the QMF. The sputtering power was 115 W. The flow rate of one of the aggregation gases Ar was 100 sccm, and the other aggregation gas He was 0 sccm. The distance between the magnetron and the aperture was set at 50 mm, and the deposition time was 90 s (Fig. 1e) and 30 s (Fig. 1f).

The SERS substrate shown in Fig. 1e is composed of long Au NWs. The NWs intertwine with each other randomly into a self-supporting, continuous Au nanofilm. Because the flow rate of the carrier gas He was low (0 sccm), the time the generated Au nanoparticles spend in the aggregation region becomes longer,[50] and the probability of Au nanoparticles colliding with each other increases; thus, longer Au NWs are formed. In contrast, when the deposition time is 30 s (Fig. 1f), we get a better view to see that the SERS substrate is almost completely composed of long Au NWs, which demonstrates that the NW growth strongly depends on the collision probability of the nanoparticles, and that this collision probability can be increased by lowering the flow rate of the carrier gas.[51]

3.2 SERS homogeneity

To explore the homogeneity of the above three kinds of SERS substrates (the deposition time are all set at 90 s), 10 μL of 10^{-4} M R6G solution was dripped onto these SERS substrates, and SERS spectra were acquired from 5 different spots within each SERS substrate. The five positions on each SERS substrate were randomly selected but were roughly equally spaced in the diagonal direction of substrate. To minimize the influence of

"edge effects", the SERS spectra were not acquired from the edge positions of each SERS substrate (R6G is a dye, a deeper color can be seen on the edge of each substrate by optical microscopy attached to the Raman Instrument). From Fig. 2, it can be seen that the SERS spectra of R6G obtained from five different locations are consistent with each other in terms of their Raman shifts, as well as their relative intensities (Fig. 2a–c). Fig. 2d gives an even clearer clarification. For the vibration mode at 771 cm^{-1}, the relative standard deviations of the peak intensity were 7.9%, 7.2%, and 9.5%, as seen in Fig. 2a–c, respectively. The good homogeneity demonstrates the reliability of these SERS substrates fabricated by this versatile nanocluster fabrication technique, and makes these substrates good candidates for detecting sodium cyclamate.

3.3 EF calculation

R6G was employed as the probe molecule to calculate the EFs of the abovementioned three kinds of Au SERS substrates (the deposition time was 90 s for all the substrates). 10^{-2} M R6G solution was employed as the bulk solution, and 10 μL of 10^{-4} M of R6G solution was dripped onto these three SERS substrates, respectively. The EF values are calculated using the equation:

$$\mathrm{EF} = \frac{I_{\mathrm{surf}}}{I_{\mathrm{bulk}}} \times \frac{N_{\mathrm{bulk}}}{N_{\mathrm{surf}}}$$

where I_{surf} and I_{bulk} are the Raman intensities of R6G molecules adsorbed on Au SERS substrate and from a 10^{-2} M of R6G solution, respectively. N_{surf} and N_{bulk} are the corresponding number of R6G molecules on the Au SERS substrate and in the bulk solution effectively illuminated by the laser beam, respectively, where N_{bulk} is calculated using the equation:

$$N_{\mathrm{bulk}} = Ahc_{\mathrm{bulk}}N_{\mathrm{A}}$$

where A is the area of the laser focal spot, c_{bulk} is the concentration of R6G bulk solution, $c_{\mathrm{bulk}} = 10^{-2}$ M, N_{A} is the Avogadro constant, h is the confocal depth of the laser, h is 13 μm.[40]

Provided that R6G molecules were in monolayer adsorption on the Au SERS substrate:

$$N_{\mathrm{surf}} = \frac{c_{\mathrm{surf}}vN_{\mathrm{A}}A}{\pi r^2}$$

where c_{surf} is the concentration of R6G solution for SERS, $c_{\mathrm{surf}} = 10^{-4}$ M, v is the volume of R6G solution used for SERS detection, $v = 10$ μL, r is the radius of 10 μL of R6G solution formed on the Au SERS substrate, $r = 3.5$ mm.

Fig. 3a and b show the normal Raman spectrum of 10^{-2} M R6G solution and the SERS spectrum of 10^{-4} M R6G solution acquired from the SERS substrate composed of Au nanoparticles, respectively. The integrated intensities of the bands for I_{bulk} (1513 cm^{-1}) and I_{surf} (1508 cm^{-1}) are 476 and 14 494 cps, respectively. Considering the different power of the

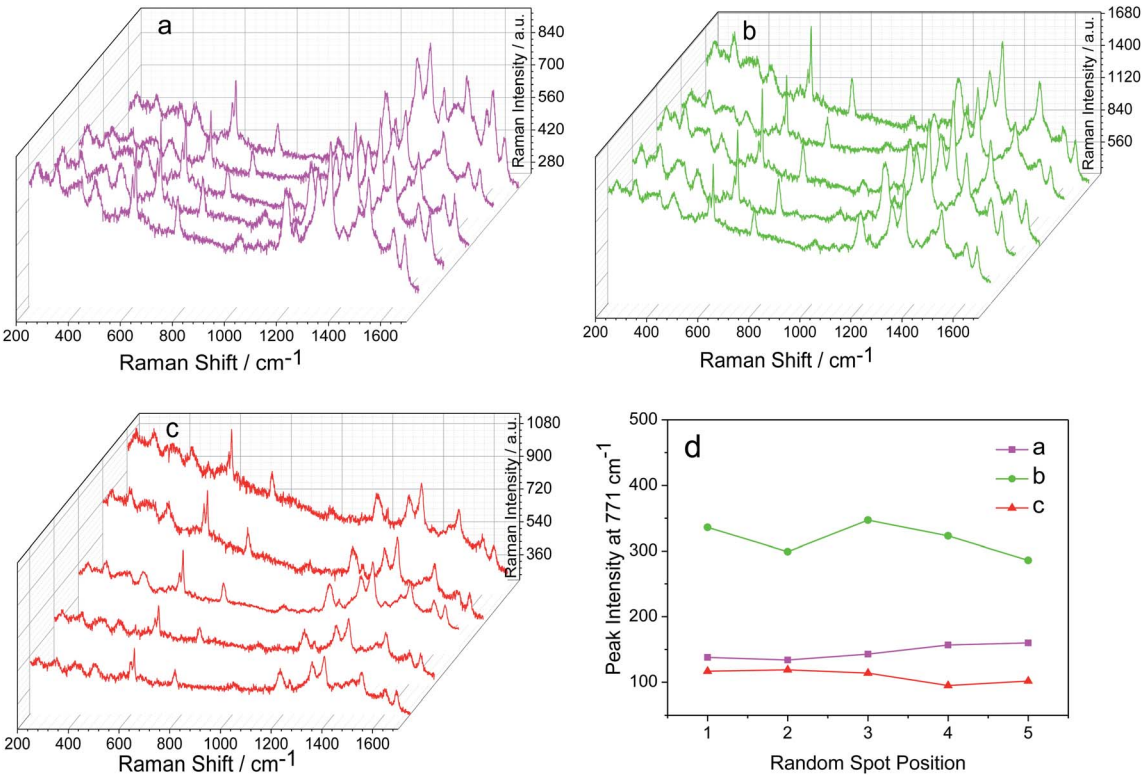

Fig. 2 SERS spectra of 10^{-4} M R6G measured at 5 random spots on the SERS substrate composed of (a) Au nanoparticles; (b) short Au NWs, with small Au nanoparticles filled in the nanogaps (deposition time is 90 s); (c) long Au NWs (deposition time is 90 s). Excitation wavelength: 785 nm; laser power: 0.8 mW; and where the collection time is 15 s exposure time and three times accumulation for each spectrum; (d) plots of the peak intensity of R6G at 771 cm^{-1} from 5 random spots on the three SERS substrates.

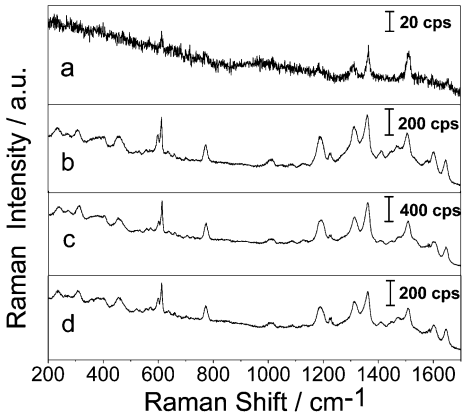

Fig. 3 (a) Normal Raman spectrum of 10^{-2} M R6G solution. Laser power: 80 mW. SERS spectrum of 10^{-4} M of R6G solution acquired from the SERS substrate composed of (b) Au nanoparticles; (c) short Au NWs with small Au nanoparticles filled in the nanogaps (deposition time is 90 s); and (d) long Au NWs (deposition time is 90 s). Laser power: 0.8 mW.

incident laser and the different number of molecules in unit volume,[40] $I_{surf}/I_{bulk} = 14\ 494 \times 10^4/476$.

Finally, the EF of this Au SERS substrate composed of Au nanoparticles (Fig. 1b) can be calculated as 1.52×10^6.

The integrated intensity of the band for I_{surf} (1512 cm^{-1}) and I_{surf} (1511 cm^{-1}) in Fig. 3c and d are 20 602 and 11 969 cps, respectively. Similarly, the EF of the SERS substrate composed of the short Au NWs with small Au nanoparticles filled in the nanogaps (Fig. 1c) can be calculated as 2.16×10^6, and the EF of the SERS substrate composed of long Au NWs (Fig. 1e) can be calculated as 1.26×10^6. Each SERS spectrum in Fig. 3b–d is an average result of the five detections in Fig. 2a–c.

Table 1 gives a brief summary regarding the SERS substrate preparation variables and EFs of the abovementioned three typical Au SERS substrates (deposition time is 90 s).

3.4 Enhancement mechanism for the abovementioned three kinds of SERS substrates

According to the results in Fig. 3, the SERS substrate composed of the short Au NWs, with small Au nanoparticles filled in the nanogaps has the highest EF; next is the SERS substrate composed of Au nanoparticles; and finally the SERS substrate with the constitution of long Au NWs with the lowest relative EF. The EFs of these three substrates are close but still have small differences, which may result from the intrinsically different nanostructures. When the short Au NWs pile up together, lots of nanogaps will be formed. At the same time, a large amount of small Au nanoparticles filled in these nanogaps will shorten the interparticle distance, which creates more hot spots and is beneficial for SERS enhancement. A similar result can be found in Qian's paper, which demonstrated that nanoporous gold film decorated by gold nanoparticles exhibits 2.9×10^7 augmentation in comparison with pure nanoporous gold film without any nanoparticle conjugation.[52] The substrate composed of Au nanoparticles is also ideal for SERS enhancement; however, the Au nanoparticles are not closely packed enough to make as many hot spots as with the small Au nanoparticles filled in the nanogaps. Therefore, the EF of this substrate composed of Au nanoparticles decreases slightly. For the SERS substrate composed of interlaced long Au NWs, the longer the NWs are, the less closely they pile up, and the larger the interparticle spacing will tend to be. Therefore, in this model, the interparticle distance is enlarged, and the number of hot spots is reduced. Therefore, the EF of the SERS substrate composed of long Au NWs is the lowest.

3.5 Long-term stability

Furthermore, the long-term stability of the three Au SERS substrates (the deposition time was 90 s for all the substrates) was also investigated. In this work, these three Au SERS substrates were kept in commercial aluminum foil separately in

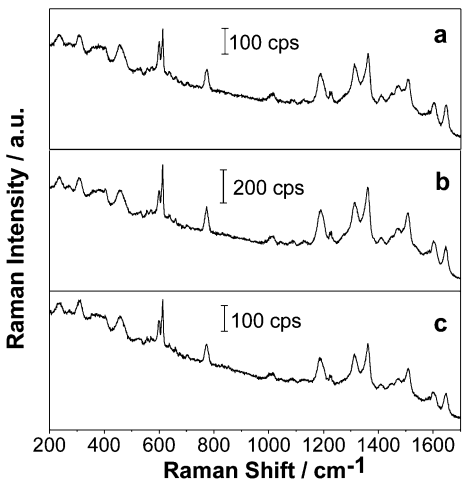

Fig. 4 SERS spectrum of 10^{-4} M of R6G solution acquired from (a) Au nanoparticles; (b) short Au NWs, with small Au nanoparticles filled in the nanogaps (deposition time is 90 s); and (c) long Au NWs (deposition time is 90 s) after they were saved in commercial aluminum foil for 110 days in the dark at room temperature. Laser power: 0.8 mW.

Table 1 Fabrication parameters and EFs of the three typical Au SERS substrates

SERS substrate	QMF	Sputtering power/W	Flow rate of Ar/sccm	Flow rate of He/sccm	Aggregation length/mm	EF
Au nanoparticles (NPs)	On	115	100	30	50	1.52×10^6
Au NWs with small Au NPs filled in the nanogaps	Off		100	30		2.16×10^6
Long intertwined Au NWs	Off		100	0		1.26×10^6

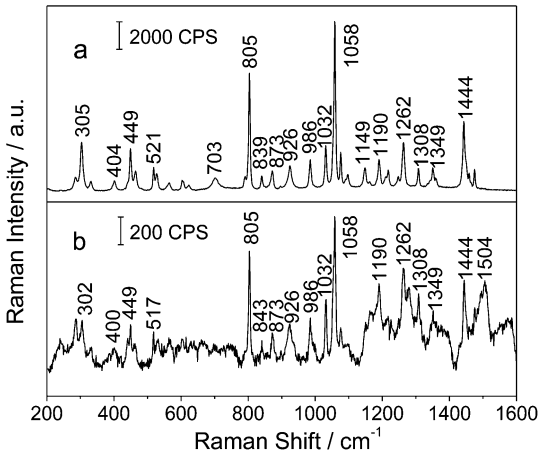

Fig. 5 The SERS spectrum of 0.1 M of sodium cyclamate acquired from (a) the substrate composed of short Au NWs, with small Au nanoparticles filled in the nanogaps; and (b) the plain and dense gold film substrate prepared by the sputter coating technique (40 mA, 150 s). Excitation wavelength: 785 nm; laser power: 8 mW. The collected time is 15 s exposure time and 3 scans.

the dark at room temperature over a period of 110 days, and were then carefully removed for stability measurements. R6G was selected as the probe molecules. Each SERS spectrum in Fig. 4 is an average result of five detections within the substrate. The five detections were randomly selected but were roughly equally spaced in the diagonal direction of the substrate. Similarly, the SERS spectra were not acquired from the edge region of each SERS substrate to minimize the influence of "edge effects". After 110 days, the enhancement of SERS substrates composed of Au nanoparticles (Fig. 4a), short Au NWs with small Au nanoparticles filled in the nanogaps (Fig. 4b), and long Au NWs (Fig. 4c) were reduced by 38.9%, 43.8%, and 37.7%, respectively (average results of the vibration mode at 771 cm^{-1} and 1189 cm^{-1}), compared to the SERS spectra obtained from freshly prepared substrates (Fig. 3b–d), which demonstrate the long-term stability of the three Au SERS substrates. The inactive property of Au together with the appropriate storage conditions keeping the Au SERS substrates from contamination are the two main reasons for the long-term stability.

3.6 SERS Detection of sodium cyclamate

Among the three kinds of SERS substrates, the one with the highest EF was selected and successfully acquired the SERS spectrum of 0.1 M of sodium cyclamate (Fig. 5a). The vibrational information of sodium cyclamate is provided in Fig. 5a, and can be used as the reference for identifying the incorrect addition of this chemical. Compared to the substrates we fabricated in the previous work by the chemical method,[40] the SERS substrate produced in this work using physical methods has an obvious advantage, *i.e.* it does not need the subtraction of substrate interference because there is no contamination from the reagents, which makes this technique an ideal approach for fabricating SERS-active substrates for fast detection. Fig. 5b is an SERS spectrum of 0.1 M sodium cyclamate acquired from the plain and dense gold film substrate prepared by a common physical fabrication technique (sputter coating). Comparing these two spectra in Fig. 5, the major Raman shifts are consistent with each other, while the plain and dense gold film substrate gives a relatively low SERS enhancement, about 10 times lower than the SERS intensity acquired from the substrate composed of short Au NWs, with small Au nanoparticles filled in the nanogaps.

3.7 Relationship between SERS intensity and sodium cyclamate concentration

Next, to evaluate the sensitivity of this food additive with the SERS substrate, a series of SERS spectra of sodium cyclamate under different concentrations were detected. 10 μL of each concentration (10^{-9} M to 10^{-1} M) was dripped onto the SERS substrate with the highest EF, and after they dried under

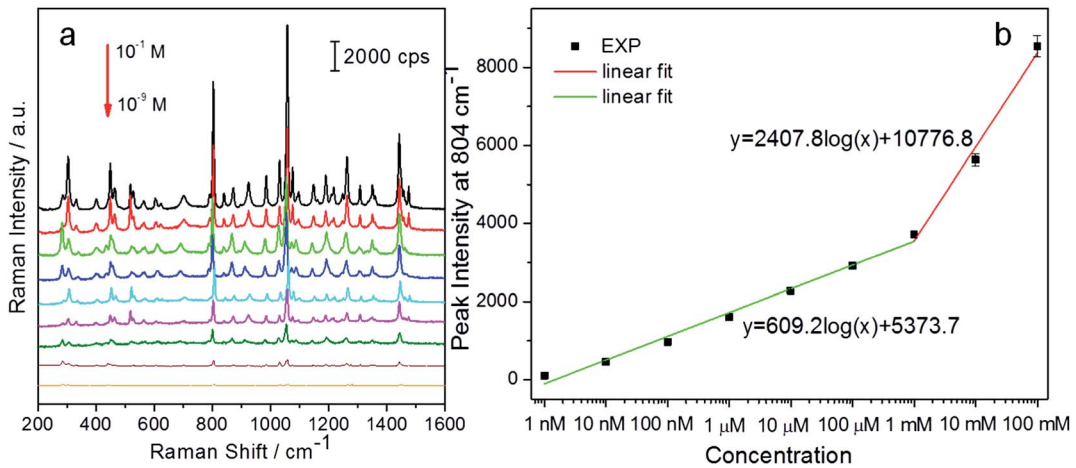

Fig. 6 (a): Concentration-dependent SERS spectra for sodium cyclamate detection (10^{-1} M to 10^{-9} M), which were obtained from the SERS substrate composed of short Au NWs with small Au nanoparticles filled in the nanogaps. Excitation wavelength: 785 nm; laser power: 8 mW; and (b) piecewise linearity plots of SERS intensity of sodium cyclamate at 804 cm^{-1} *vs.* sodium cyclamate concentration.

ambient conditions, the SERS spectra were acquired (Fig. 6a). In Fig. 6a, the SERS spectra of sodium cyclamate were obtained, and it can be seen that the spectral intensity decreases as the concentration decreases.

Fig. 6b is the correlation between the SERS intensity and sodium cyclamate concentration. The SERS peak intensity of sodium cyclamate at 804 cm^{-1} was set as the *y*-axis, and the sodium cyclamate concentration was set as the *x*-axis. Similar to the result in our previous paper,[37] two linear regions exist in the whole concentration range. When the sodium cyclamate concentration is in the range of 10^{-3} to 10^{-1} M, the linear regression equation is $y = 2407.8 \log(x) + 10776.8$, and the correlation coefficient is 0.993 ($n = 3$). When the sodium cyclamate concentration is in the range of 10^{-9} to 10^{-3} M, the linear regression equation is $y = 609.2 \log(x) + 5373.7$, and the correlation coefficient is 0.995 ($n = 7$). The detection limit of sodium cyclamate can be calculated as 1.6×10^{-9} M, according to the signal/noise ratio of three.

4. Conclusions

In this work, we introduced a versatile nanocluster fabrication technique to prepare Au SERS-active substrates, which allows the pre-selection of the nanocluster size. Three typical SERS substrates, with the compositions of Au nanoparticles, short Au NWs with small Au nanoparticles filled in the nanogaps, and long Au NWs intertwined into a self-supporting film, were fabricated respectively by this system under different parameters. These three SERS substrates have good homogeneity, long-term stability, and their EFs are all in the order of 10^6 using R6G as probe molecules. Then the SERS spectrum of sodium cyclamate, a food additive, was successfully acquired from the SERS substrate with the highest EF, which was the one composed of small Au nanoparticles distributed around short Au NWs, with a SERS intensity 10 times higher than the SERS intensity obtained from the plain and dense Au film substrate prepared by a common physical fabrication technique. Finally, the correlation between the SERS intensity and sodium cyclamate concentration was given, and a set of piecewise-linear equations were also provided with a detection limit of 1.6×10^{-9} M. This technique is time-efficient, easily to prepares large-area SERS substrates with tunable nanostructures, and can also produce chemically clean SERS substrates, which suggests that this versatile nanofabrication technique is promising for reliable SERS substrates fabrication, and has potential application of producing SERS substrates for the detection of chemical molecules.

Acknowledgements

We thank Ronald Gary, Casey Hall-Wheeler, and Shirley Shen from UNLV for assistance with ultrapure water. This work was supported by the National Natural Science Foundation of China (no. 50871028) and the Fundamental Research Funds for the Central Universities (no. N110610001). G. W. Qin appreciates Program for New Century Excellent Talents in University (no. NCET-10-0272). J. Chen appreciates the assistance from China Scholarship Council (CSC), and Northeastern University excellent doctoral dissertation breeding program, China.

References

1 R. S. Golightly, W. E. Doering and M. J. Natan, *ACS Nano*, 2009, **3**, 2859–2869.
2 J. P. Camden, J. A. Dieringer, J. Zhao and R. P. Van Duyne, *Acc. Chem. Res.*, 2008, **41**, 1653–1661.
3 E. C. Le Ru and P. G. Etchegoin, *Principles of Surface Enhanced Raman Spectroscopy and Related Plasmonic Effects*, Elsevier, Amsterdam, Netherlands, 2009.
4 S. M. Nie and S. R. Emory, *Science*, 1997, **275**, 1102–1106.
5 K. Kneipp, Y. Wang, H. Kneipp, L. T. Perelman, I. Itzkan, R. Dasari and M. S. Feld, *Phys. Rev. Lett.*, 1997, **78**, 1667–1670.
6 C. Qian, C. Ni, W. X. Yu, W. G. Wu, H. Y. Mao, Y. F. Wang and J. Xu, *Small*, 2011, **7**, 1801–1806.
7 A. Barhoumi and N. J. Halas, *J. Am. Chem. Soc.*, 2010, **132**, 12792–12793.
8 S. Lal, N. K. Grady, J. Kundu, C. S. Levin, J. B. Lassiter and N. J. Halas, *Chem. Soc. Rev.*, 2008, **37**, 898–911.
9 K. M. Mayer and J. H. Hafner, *Chem. Rev.*, 2011, **111**, 3828–3857.
10 W. Lee, S. Y. Lee, R. M. Briber and O. Rabin, *Adv. Funct. Mater.*, 2011, **21**, 3424–3429.
11 E. A. Vitol, Z. Orynbayeva, M. J. Bouchard, J. Azizkhan-Clifford, G. Friedman and Y. Gogotsi, *ACS Nano*, 2009, **3**, 3529–3536.
12 A. Matschulat, D. Drescher and J. Kneipp, *ACS Nano*, 2010, **4**, 3259–3269.
13 A. Pallaoro, G. B. Braun and M. Moskovits, *Proc. Natl. Acad. Sci. U. S. A.*, 2011, **108**, 16559–16564.
14 J. Theiss, P. Pavaskar, P. M. Echternach, R. E. Muller and S. B. Cronin, *Nano Lett.*, 2010, **10**, 2749–2754.
15 X. M. Qian, X. H. Peng, D. O. Ansari, Q. Yin-Goen, G. Z. Chen, D. M. Shin, L. Yang, A. N. Young, M. D. Wang and S. M. Nie, *Nat. Biotechnol.*, 2008, **26**, 83–90.
16 G. F. Wang, R. J. Lipert, M. Jain, S. Kaur, S. Chakraboty, M. P. Torres, S. K. Batra, R. E. Brand and M. D. Porter, *Anal. Chem.*, 2011, **83**, 2554–2561.
17 R. A. Halvorson and P. J. Vikesland, *Environ. Sci. Technol.*, 2010, **44**, 7749–7755.
18 K. V. Kong, Z. Y. Lam, W. K. O. Lau, W. K. Leong and M. Oivo, *J. Am. Chem. Soc.*, 2013, **135**, 18028–18031.
19 X. M. Qian, X. Zhou and S. M. Nie, *J. Am. Chem. Soc.*, 2008, **130**, 14934–14935.
20 S. P. Liu, N. Chen, L. X. Li, F. F. Pang, Z. Y. Chen and T. Y. Wang, *Opt. Mater.*, 2013, **35**, 690–692.
21 S. J. Kundu, *J. Mater. Chem. C*, 2013, **1**, 831–842.
22 S. Kundu and M. Jayachandran, *RSC Adv.*, 2013, **3**, 16486–16498.
23 G. S. Hong, C. Li and L. M. Qi, *Adv. Funct. Mater.*, 2010, **20**, 3774–3783.
24 S. Chang, Z. A. Combs, M. K. Gupta, R. Davis and V. V. Tsukruk, *ACS Appl. Mater. Interfaces*, 2010, **2**, 3333–3339.

25 M. Bechelany, P. Brodard, J. Elias, A. Brioude, J. Michler and L. Philippe, *Langmuir*, 2010, **26**, 14364–14371.
26 X. Z. Ye and L. M. Qi, *Nano Today*, 2011, **6**, 608–631.
27 J. Paczesny, A. Kaminska, W. Adamkiewicz, K. Winkler, K. Sozanski, M. Wadowska, I. Dziecielewski and R. Holyst, *Chem. Mater.*, 2012, **24**, 3667–3673.
28 M. S. Chen, I. Y. Phang, M. R. Lee, J. K. W. Yang and X. Y. Ling, *Langmuir*, 2013, **29**, 7061–7069.
29 R. Gunawidjaja, E. Kharlampieva, I. Choi and V. V. Tsukruk, *Small*, 2009, **5**, 2460–2466.
30 S. J. Lee, J. M. Baik and M. Moskovits, *Nano Lett.*, 2008, **8**, 3244–3247.
31 S. J. Guo, S. J. Dong and E. K. Wang, *Cryst. Growth Des.*, 2009, **9**, 372–377.
32 H. Wang, C. S. Levin and N. J. Halas, *J. Am. Chem. Soc.*, 2005, **127**, 14992–14993.
33 A. Tao, F. Kim, C. Hess, J. Goldberger, R. R. He, Y. G. Sun, Y. N. Xia and P. D. Yang, *Nano Lett.*, 2003, **3**, 1229–1233.
34 C. F. Chen, J. M. Hao, L. Y. Zhu, Y. Q. Yao, X. G. Meng, W. Weimer and Q. W. K. Wang, *J. Mater. Chem. A*, 2013, **1**, 13496–13501.
35 E. M. Freer, O. Grachev, X. F. Duan, S. Martin and D. P. Stumbo, *Nat. Nanotechnol.*, 2010, **5**, 525–530.
36 X. Y. Zhang, A. M. Hu, T. Zhang, W. Lei, X. J. Xue, Y. H. Zhou and W. W. Duley, *ACS Nano*, 2011, **5**, 9082–9092.
37 J. Chen, G. W. Qin, J. S. Wang, J. Y. Yu, B. Shen, S. Li, Y. P. Ren, L. Zuo, W. Shen and B. Das, *Biosens. Bioelectron.*, 2013, **44**, 191–197.
38 W. E. Smith, *Chem. Soc. Rev.*, 2008, **37**, 955–964.
39 J. Y. Huang, C. Zong, L. J. Xu, Y. Cui and B. Ren, *Chem. Commun.*, 2011, **47**, 5738–5740.
40 J. Chen, B. Shen, G. W. Qin, X. W. Hu, L. H. Qian, Z. W. Wang, S. Li, Y. P. Ren and L. Zuo, *J. Phys. Chem. C*, 2012, **116**, 3320–3328.
41 A. Banerjee and B. Das, *Rev. Sci. Instrum.*, 2008, **79**, 033910.
42 M. Culha, B. Cullum, N. Lavrik and C. K. Klutse, *J. Nanotechnol.*, 2012, 971380.
43 M. R. Weihrauch and V. Diehl, *Ann. Oncol.*, 2004, **15**, 1460–1465.
44 I. F. Gaunt, M. Sharratt, P. Grasso, A. B. G. Lansdown and S. D. Gangolli, *Food Cosmet. Toxicol.*, 1974, **12**, 609–624.
45 R. W. James, R. Heywood and D. Crook, *Food Cosmet. Toxicol.*, 1981, **19**, 291–296.
46 A. Roberts and A. G. Renwick, *Toxicol. Appl. Pharmacol.*, 1989, **98**, 230–242.
47 A. Roberts, A. G. Renwick, G. Ford, D. M. Creasy and I. Gaunt, *Toxicol. Appl. Pharmacol.*, 1989, **98**, 216–229.
48 S. Armenta, S. Garrigues and M. de la Guardia, *Anal. Chim. Acta*, 2004, **521**, 149–155.
49 http://www.oaresearch.co.uk.
50 B. Das and A. Banerjee, *Nanotechnology*, 2007, **18**, 445202.
51 A. N. Banerjee, R. Krishna and B. Das, *Appl. Phys. A*, 2008, **90**, 299–303.
52 L. H. Qian, B. Das, Y. Li and Z. L. Yang, *J. Mater. Chem.*, 2010, **20**, 6891–6895.